ADVANCED FUNCTIONAL MATERIALS
www.afm-journal.de



# Hexagonal Boron Nitride and Graphite Oxide Reinforced Multifunctional Porous Cement Composites

*Mohammad A. Rafiee, Tharangattu N. Narayanan, Daniel P. Hashim, Navid Sakhavand, Rouzbeh Shahsavari, Robert Vajtai, and Pulickel M. Ajayan**

**The synthesis and characterization of multifunctional cement and concrete composites filled with hexagonal boron nitride (h-BN) and graphite oxide (GO), is reported and their superior mechanical strength and oil adsorption properties compared to composites devoid of fillers are illustrated. GO is utilized to bridge the cement surfaces while h-BN is used to mechanically reinforce the composites and adsorb the oil. Introduction of these fillers even at low filler weight fractions increases the compressive strength and toughness properties of pristine cement and of porous concrete significantly, while the porous composite concrete illustrates excellent ability for water separation and crude oil adsorption. Experimental results along with theoretical calculations show that such nanoengineered forms of cement based composites would enable the development of novel forms of multifunctional structural materials with a range of environmental applications.**

## 1. Introduction

Boron nitride (BN) exists in various crystalline forms, along with its hexagonal allotrope, h-BN similar to that of graphite structure.[1] The 2D crystal structure of h-BN exhibits unique features, such as thermodynamic (air stable up to 1000 °C) and chemical stability,[2] excellent mechanical strength[3] as well as a layered nature, and highly electrical insulating, while its highly thermally conducting nature makes it suitable for many technological applications. The hydrophobic nature of h-BN sheets can be utilized for making non-wetting surfaces, underwater constructions, or even filtration systems. The commercial products of h-BN include various thermal management materials such as thermal grease, thermal pads, coatings, and cosmetics.[4] h-BN is widely used in cosmetics due to its oil adsorption capacity and IR-radiation absorption capability. Recently, exfoliated h-BN sheets were demonstrated for applications as additives in transformer oils for thermal management applications.[5]

Dr. M. A. Rafiee, Dr. T. N. Narayanan, D. P. Hashim, Dr. R. Vajtai, Prof. P. M. Ajayan
Department of Mechanical Engineering and Materials Science
Rice University
6100 Main Street, Houston, TX 77006, USA
E-mail: ajayan@rice.edu
N. Sakhavand, Prof. R. Shahsavari
Department of Civil and Environmental Engineering
Rice University
Houston, TX 77005, USA

**DOI: 10.1002/adfm.201203866**

Recently, the occurrence of oil spills has become a major environmental threat that directly affects the ecosystem.[6,7] For oil remediation, a broad variety of materials such as adsorbents, solidifiers, dispersants, and skimmers have been used,[6,7] but the availability of an eco-friendly and efficient approach is still lacking. Various attempts were made in the past to separate and remove oil from water. Most of these techniques were based on the selective oil adsorption capacity of polymers or membrane based filtration.[8–10] In most cases, the hydrophobic properties of these materials are used to separate oil from water. Each polymer has a saturation limit for its adsorption capacity, while the efficiency of membrane-based separation is limited to low fluent rates.[11]

Similar to h-BN, other 2D materials such as graphene or graphene-oxide-containing composites have been proven to have significantly enhanced mechanical properties in composite materials.[12,13] Addition of more than one nanocarbon in a polymer matrix is also found to enhance the resultant mechanical properties of composites to a large extent.[14] Recently, Walker et al. reported a giant enhancement in the toughness of graphene platelet (GPL; thermally reduced graphite oxide) based ceramic composites.[15] The fracture toughness enhancement of such ceramic composites is associated with the mechanism of anchoring and wrapping the GPL fillers underneath the silica grains, therefore forming a continuous wall of GPL fillers along the grain boundaries that arrests crack propagation in three dimensions rather than two dimensions. Graphite and h-BN, with their relatively similar structures, are used to synthesize various forms of carbon nanotubes (CNTs) and boron nitride nanotubes (BNNTs). Despite the differences in the electronic properties of CNTs and BNNTs, similar mechanical properties specifically in the Young's modulus are reported in these materials, demonstrating potential applications such as mechanical reinforcement.[16] Ultrathin boron nitride sheets can improve the mechanical properties of BN-based polymer composites. As an example, addition of ≈0.3 wt% BN nanosheets to poly(methyl methacrylate) (PMMA) increases the elastic modulus and strength by ≈22% and ≈11%, respectively.[3] Recently, Rao et al. reported the mechanical property modulation of PMMA with BN nanoflakes and the BN layer dependency on the enhancement of stiffness and hardness of PMMA–BN composites.[17] PMMA–BN composites showed enhanced mechanical properties when the number of BN

layers was less and the high surface area in few layered h-BN provides a high interaction cross-section with the polymer and contributes to enhanced mechanical properties.

Porous concretes, also called pervious concretes, are structures of high porosity used for applications[18,19] in sustainable construction, greenhouses, and storm-water management. By using h-BN and GO fillers, the goal is not only to engineer and fabricate porous composite concretes with excellent mechanical properties, but also to enhance the oil adsorption capacity of such composite materials for underwater construction structures having oil spill mitigation properties. Such structures could also be useful for water-gas-oil-sand separation with improved phase separation and enhanced water quality. Here, we report the use of h-BN nanoflakes with cement and concrete composites for the efficient hydrocarbon (crude oil) adsorption and heavy crude oil/water separation. This concrete-based material has higher volumetric adsorption capacity while keeping a high water fluent rate. Mechanical studies proved the reinforcement capacity of h-BN flakes meanwhile, the graphite oxide (GO), with its rich verity of functional group, is used to bridge cement turbermorite sheets. A theoretical simulation is used to demonstrate this bridging mechanism that helps to keep the silicate gel layers closer, thereby helping to remove hydrocarbons successfully even with a low filler fraction of h-BN.

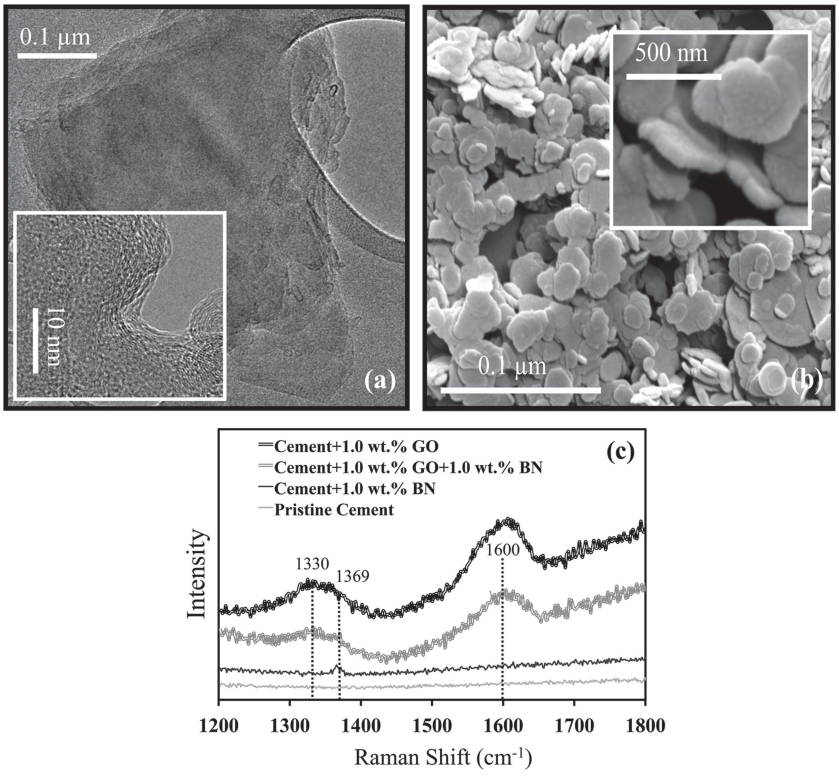


**Figure 1.** a) TEM image of synthesized GO flakes deposited on top of TEM grid after sonication for 6 h in water. b) SEM image of BN powders deposited on top of the silicon wafer. c) Raman analysis of pristine cement and the composites with cement with BN and GO fillers.

## 2. Results and Discussion

### 2.1. Synthesis of BN and GO Cement and Concrete Composites

GO was synthesized using modified Hummer's procedure[20–22] (details are reported in the Experimental Section; **Figure 1**) and h-BN sheets were procured from Sigma Aldrich (≈500 nm to 1 μm lateral width and 80–100 nm thickness, 98% pure). The protocol employed to disperse BN and GO fillers in pristine cement and porous concrete are provided in the Experimental Section. ASTM C39 standard uniaxial (static) compression tests were conducted on cylindrical coupons to study the mechanical properties of the composites. We determined the compressive strength and toughness of the composites in comparison to the baseline (pristine) cement/concrete without any filler.

Figure 1a shows a transmission electron microscopy (TEM) and high-resolution TEM (HRTEM; inset) images of a GO flake synthesized via modified Hummers technique. The HRTEM image shows the edge of a GO flake shows the structure of several layers of graphene oxide. Figure 1b is a scanning electron microscopy (SEM) image of h-BN flakes deposited on a silicon. Figure 1c shows the Raman spectra analysis for pristine cement and composites with ≈1.0 wt% GO (hereafter named GO cement) and ≈1.0 wt% h-BN (BN cement). Pristine cement shows no Raman active modes while GO cement depicts clear peaks at ≈1330 $cm^{-1}$ and ≈1600 $cm^{-1}$ corresponding to D (disorder) and G (order) peaks of graphite oxide, respectively.[23] In the case of BN cement, the Raman analysis indicates a peak at ≈1369 $cm^{-1}$ corresponding to the $E_{2g}$ mode of B–N vibration and also showing other peaks that corresponding to GO.

The as-produced GO and commercial h-BN sheets were dispersed in cement and concrete by ultrasonication and ball milling techniques (see Experimental Section). To study the mechanical properties of the composites, the cylindrical coupons (height to diameter ratio of 2:1) were fabricated according to the ASTM C39 standard, and static compression tests were carried out using an Instron universal testing machine. **Figure 2**a,b show SEM images of the fractured surface of the h-BN and GO cements. Figure 2a shows the uniform dispersion of h-BN fillers in the cement matrix. Figure 2b shows the GO bridging mechanism along the cement particles; no indication of large agglomeration or clustering of the fillers in the cement and concrete composites (containing both cement and gravels) is observed from the fracture surfaces.

First, to study the reinforcing effect of h-BN and GO fillers in pure cement, static compression tests on cylindrical specimens (7 cm in diameter and 14 cm in height) of these composites were carried out at a loading rate of ≈1.5 MPa/min at room temperature (≈24°C). **Figure 3**a depicts the comressive stress vs strain response of the pure cement and reinforced h-BN and

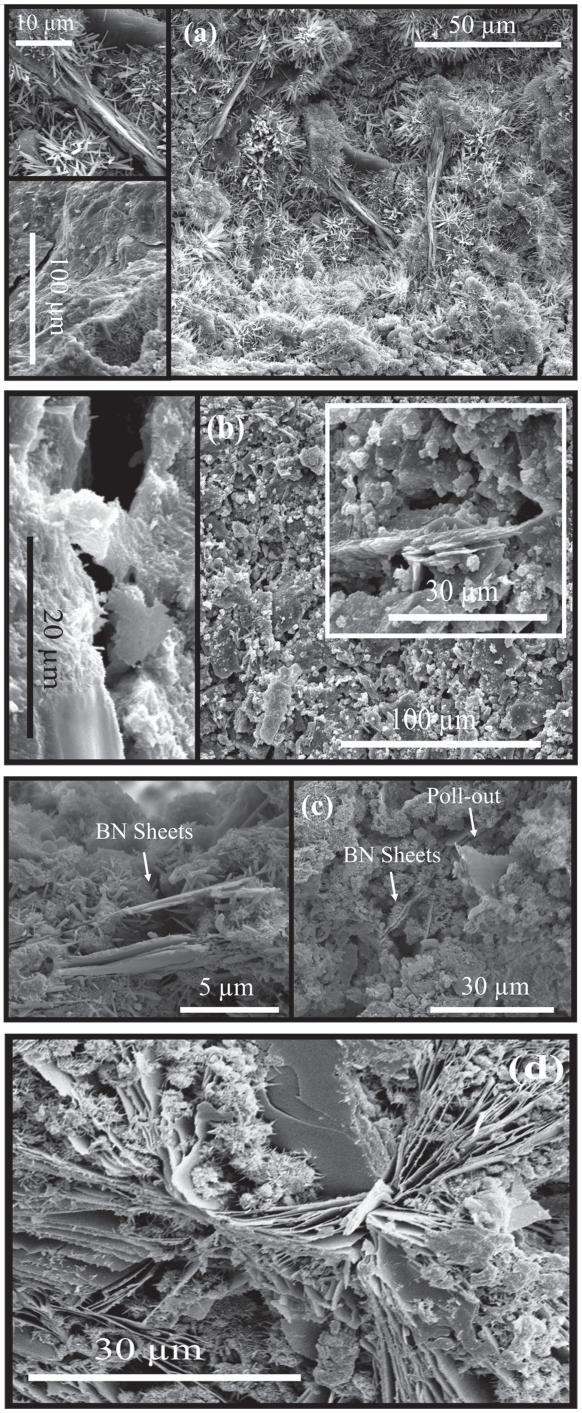


**Figure 2.** Typical SEM images of fracture surface of cement composites with a) ≈1.0 wt% of BN fillers illustrating the uniform dispersion of fillers (flat flakes in the picture) in the cement matrix (needle-like particle in the picture) and b) ≈1.0% of GO fillers depicting the bridging mechanism along the cement particles. No indication of large agglomeration or clustering of the fillers in the cement and concrete composites is observed. c) SEM image of the 1.0 wt% BN concrete composite fractured specimen showing both BN sheet poll-out of the matrix mechanism and the strong adhesion mechanism between the BN sheets and cement particles. d) SEM image of the fracture surface of cement composite with ≈1.0 wt% of BN and ≈1.0 wt% of GO fillers illustrating the large agglomeration of fillers in the cement matrix.

GO cements. The h-BN reinforced cement illustrates a significant increase in the compressive strength (≈89% increase) and toughness (≈85% increase) compared to the pristine cement (comparing Figure 3a,b). In GO and h-BN/GO cement composites, a decrease (≈17%) and an increase (≈25%) in the compressive strength compared to pure cement, respectively, were observed. As it is seen in Figure 3c, in addition to the compressive strength, we calculated the toughness (i.e., energy absorption at failure that is the total area under the stress versus strain curve) of the pure and cement composites. Using a mixture of 1.0 wt% GO and 1.0 wt% h-BN fillers in cement significantly decreased the toughness value by ≈55% compared to baseline cement, while adding 1.0 wt% fraction of GO and h-BN fillers in composites separately, toughness increases by ≈10% and 85% compared to the pristine cement, respectively. This difference in mixed fillers can be due to the large agglomeration of fillers in the cement matrix, as is seen in Figure 2d. Additionally, incompatible natures of hydrophilic GO and hydrophobic h-BN fillers can form a very brittle structure of cement-based composites with poor interfacial filler-matrix interface during water and cement hydration process.

In order to fabricate practical cement-based composites, porous concretes are engineered by adding aggregates to cement before processing the specimens. Similarly to investigate the effect of the h-BN and GO fillers in these composites, at least four specimens for each of the materials are fabricated, and the compression tests on cylindrical coupons (12 cm in diameter and 24 cm in height) are repeated at the same loading fraction of ≈1.0 wt% h-BN and ≈1.0 wt% GO (Figure 3d,e). While the toughness in ≈1.0% h-BN concrete dramatically increased by ≈200%, the compressive strength of this composite increased by ≈64% compared to the pristine concrete (Figure 3e). Despite the fact that utilizing a mixture of 1.0 wt% GO and 1.0 wt% h-BN fillers in cement decreased the toughness of pure cement by ≈55%, the toughness value significantly increased by ≈175% in porous concrete material with same filler loading fractions. Figure 2c shows the SEM image of the 1.0 wt% BN concrete composite fractured specimen showing both BN sheet pull-out of the matrix and the strong adhesion between the BN sheets and cement particles. In general, different types of mechanisms can be seen in BN-based composites. For example, it is reported that in silicon nitride/BN composites, multilevel toughening mechanisms, including crack deflection, bifurcation, and pull-out of matrix sheets, are attributed to the enhanced toughness property of the composites.[24]

The above mentioned mechanically reinforced h-BN concrete composite (containing both gravel and cements) was tested for water-diluted bitumen crude oil mixture separation (porous concrete is widely used in pavements to drain water).[25] The photographs of the various experiment sequences involved are demonstrated in **Figure 4**a. We used Canadian bitumen heavy crude oil diluted with naphtha (1:4) and mixed 100 mL of the mixture with 400 mL of water before applying the filtration. It was found that h-BN concrete composite effectively filters the crude oil from water and the filtered water becomes clear. Both the filtrate and original water/diluted heavy oil mixture were subjected to UV-vis absorption studies. The results indicate that a major fraction of the hydrocarbon is removed while passing through the h-BN concrete composite (Figure 4b).

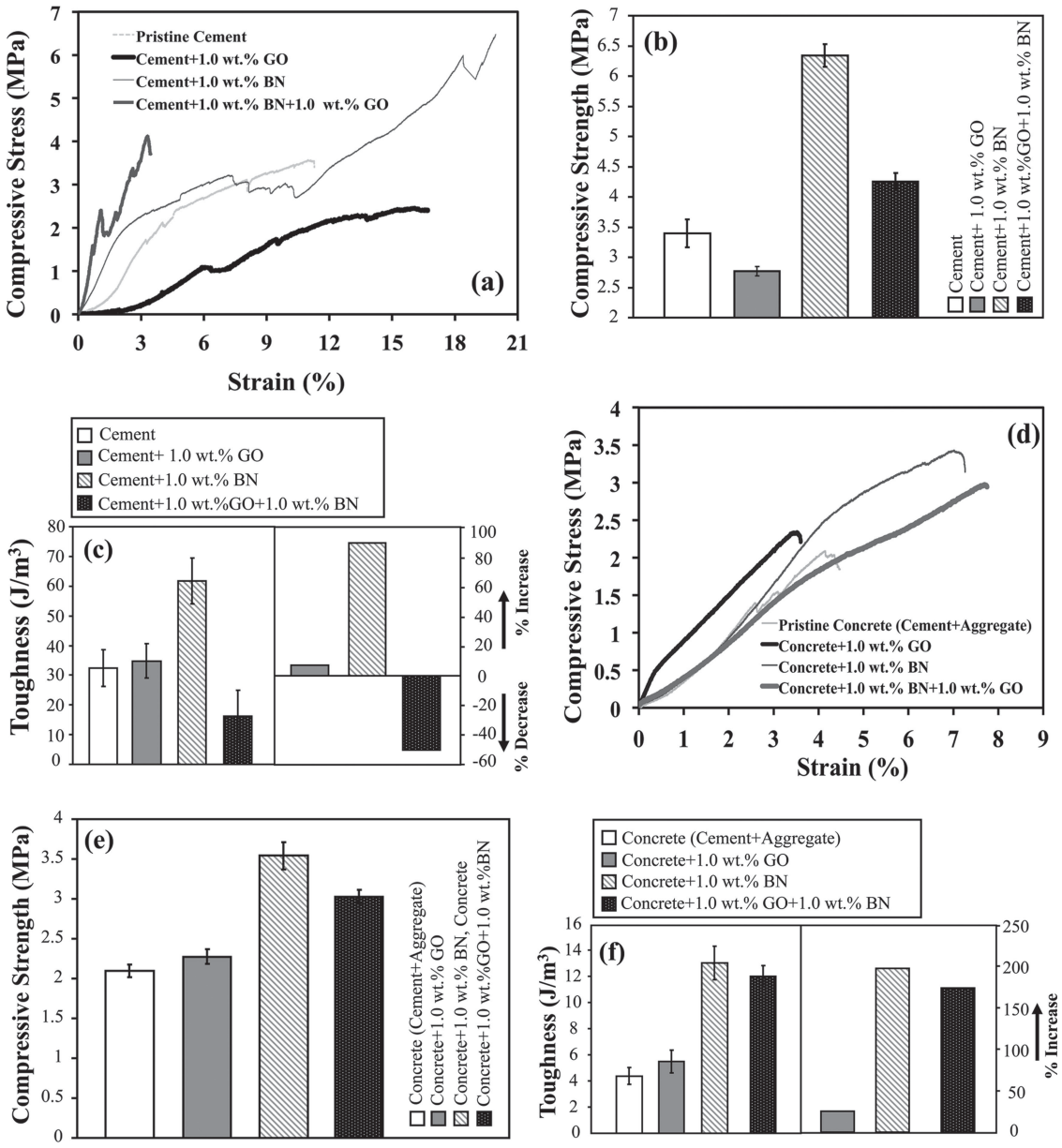


**Figure 3.** Uniaxial mode compressive testing in cement-based composites. a) Typical stress vs strain curve of the pristine cement and composite formulations with 1.0 wt% fraction of GO and h-BN fillers. b) Averaged results for the compressive strength for the baseline cement and the composites. c) Corresponding results and the percentage changes for the total area under the stress vs strain curves (i.e., toughness) for the pure cement and the composite formulations. d) Typical stress versus strain curve of the pristine porous concrete and composite formulations with 1.0 wt% fraction of GO and h-BN sheets. e) Averaged results for the compressive strength for the baseline concrete and the GO and h-BN composites. f) Corresponding results for the total area under the stress vs strain curves (i.e., toughness) for the pure cement and the composite formulations.

### 2.2. Molecular Dynamics Simulation on Hydrocarbon Absorption

The capability of h-BN flakes used to absorb the oil is shown in **Figure 5**. We used this property to apply h-BN porous concrete composites for application in heavy crude oil and water separation. As a result, in order to explore the role of h-BN in cement and concrete composites, a molecular dynamics (MD) simulation study was conducted. The computational experiment included a MD simulation of a few thousands of typical crude oil molecules confined between two surfaces of cement hydrate where one of the surfaces was coated with a single h-BN sheet (Figure 5b). The distance between the two surfaces was 205 Å. Tobermorite 11 Å[26] was used as an structural model for the basic building blocks of cement hydrate, calcium-silicate-hydrate (C-S-H) gel, which is the binder phase of concrete and the principal source of strength and durability in all Portland cement concretes.[26,27] These

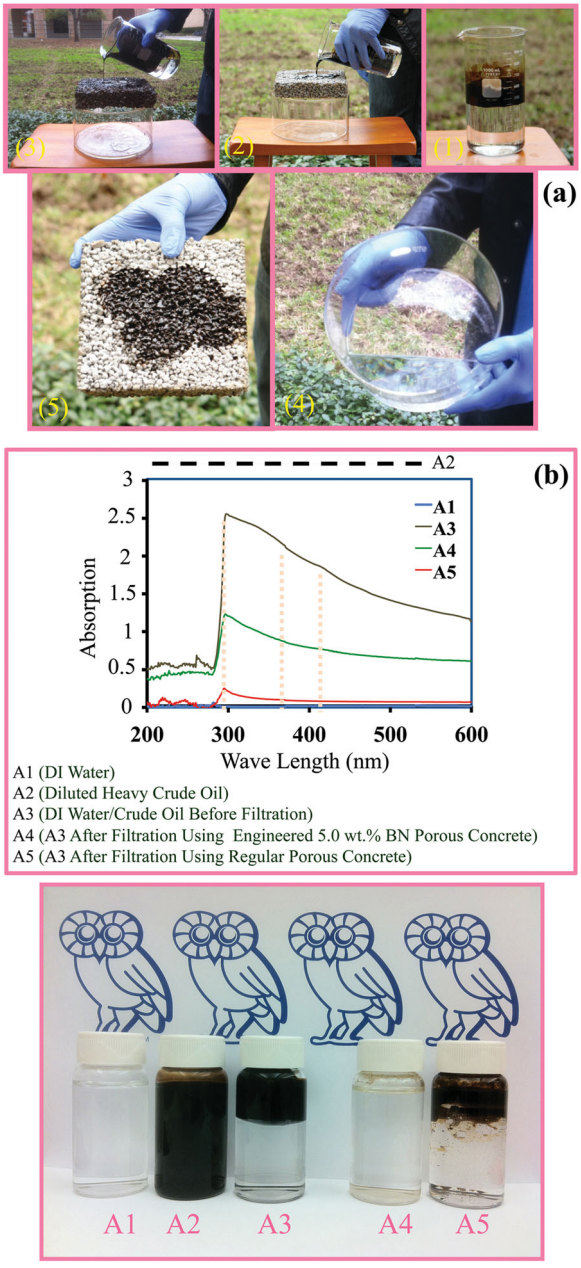


**Figure 4.** a) The photographs of the various experiments sequences involved in crude oil and water separation. The Canadian bitumen heavy crude oil was diluted with naphtha (1:4) and 100 mL of the mixture was mixed with 400 mL of water before applying the filtration. As shown, a large amount of crude oil was removed and adsorbed by the porous concrete with ≈7.0 wt% fraction of h-BN fillers. b) UV absorption analysis of water and crude oil and their mixtures before and after the filtration.

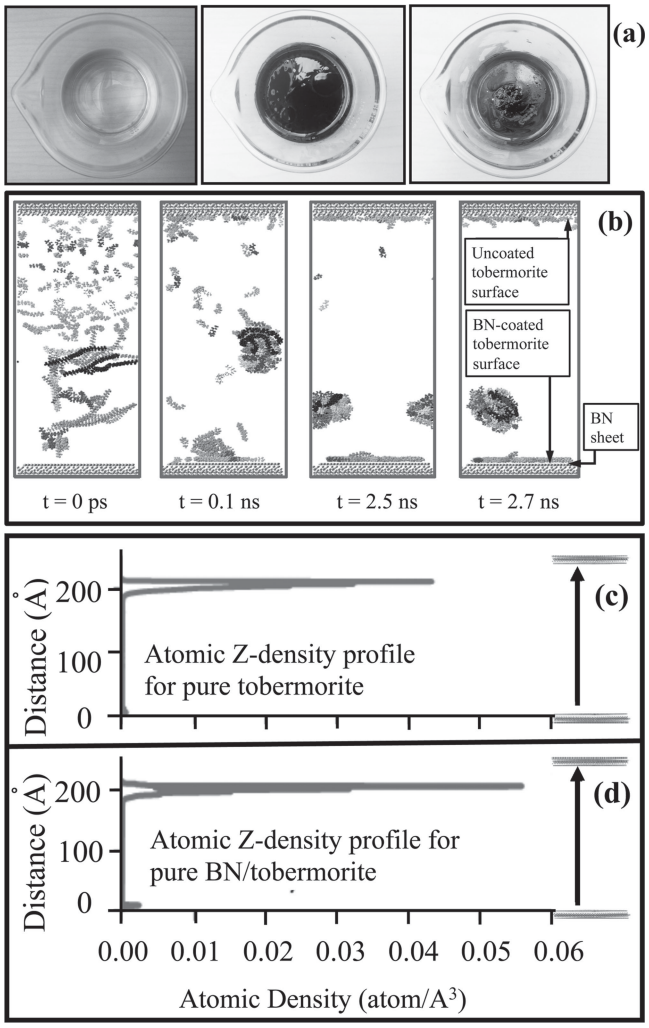


**Figure 5.** a) Experiment showing the capability of h-BN flakes used to absorb the oil. b) Snapshots of the crude oil adsorption on h-BN coated Tobermorite. Different colors show different types of hydro-arbons. Top surface is uncoated and bottom surface is coated with a single layer of h-BN sheet. c) Atomic *z*-density profile for pure Tobermorite surfaces. d) Atomic *z*-density profile for h-BN coated surfaces. In (c,d), the vertical axis represents the distance from the surface of the bottom layer, which starts from zero and increases to the top layer, located at $z = 214$ Å. The horizontal axis determines the atomic density at the given distance. The top layer in both cases adsorbs a majority of the carbon atoms.

hydrate gels can be interconnected with the help of oxygen functionalities of graphite oxide.[28] The hydrophilic GO contains number of intercalated and adsorbed water molecules. This will also help to form hydrogen bonding with cement hydrate layers.

The crude oil is generally composed of alkane chains of C6 to C30 of form $C_nH_{2n+2}$.[29,30] The composition of the *n*-alkanes in this study is summarized in **Table 1**. The tobermorite layers are restrained from movement during the simulation. The pairwise and electrostatic interaction parameters for tobermorite atoms are taken from the CSH-FF force field potential,[31] which was recently customized for the cement hydrate family. The interaction of hydrocarbon atoms are based on the consistent valance force field (CVFF),[32,33] and the BN atoms are modeled as uncharged Lennard–Jones (LJ) particles.[34] The LJ parameters for cross interactions between the crude oil atoms, BN, and tobermorite are calculated through the standard Lorentz–Berthelot combination rules.[35] MD simulations were performed using a scalable parallel molecular dynamics code, LAMMPS,[29] and VMD software[36] was used for atomistic visualization.

**Table 1.** Comparison of crude oil used in the molecular dynamics simulation.

| Species | No. in the simulation box | Species | No. in the simulation box | Species | No. in the simulation box | Species | No. in the simulation box | Species | No. in the simulation box |
|---|---|---|---|---|---|---|---|---|---|
| $C_6$ | 20 | $C_{11}$ | 20 | $C_{16}$ | 12 | $C_{21}$ | 8 | $C_{26}$ | 4 |
| $C_7$ | 21 | $C_{12}$ | 17 | $C_{17}$ | 11 | $C_{22}$ | 7 | $C_{27}$ | 5 |
| $C_8$ | 25 | $C_{13}$ | 17 | $C_{18}$ | 10 | $C_{23}$ | 6 | $C_{28}$ | 4 |
| $C_9$ | 26 | $C_{14}$ | 15 | $C_{19}$ | 9 | $C_{24}$ | 5 | $C_{29}$ | 4 |
| $C_{10}$ | 23 | $C_{15}$ | 15 | $C_{20}$ | 9 | $C_{25}$ | 5 | $C_{30}$ | 3 |

The simulation is conducted under microcanonical ensemble (NVT) at 300 K for 2.7 ns. Periodic boundary condition is applied to the system in the *x*- and *y*-directions. Figure 5b shows a few snapshots of the adsorption mechanisms at various time steps. Accordingly, it seems that at the initial stage the alkane chains are adsorbed by both the BN and tobermorite surfaces. However, over time more alkane chains (specially the light ones such as C6, C7) tend to move towards the BN surface.

To investigate the distribution of the alkane chains between the two surfaces (along the *z*-axis), the atomic *z*-density profiles are calculated. The atomic *z*-density profile, $\rho_i(z)$, of an atom type $i$ at the distance $z$ from the reference point represents the total number of atom type $i$, $\langle N_a(z, z+\Delta z)\rangle$ in a slab of thickness $\Delta z$ centered at $z$, divided by the volume of the slab:

$$\rho_i(z) = \frac{\langle N_a(z, z+\Delta z)\rangle}{S_{xy}\Delta z} \quad (1)$$

where $S_{xy}$ is the surface area of the slab and the symbol $\langle\ \rangle$ denotes the average over the simulation period. Figure 5c,d are the calculated atomic z-density profiles for all carbon atoms, which show the average location of the hydrocarbon chains along the *z*-axis of the simulation box. The profile is averaged every 4 ps. It is found that approximately 60% more carbon atoms are adsorbed by the BN-coated surface than the uncoated surface. This analysis reveals the hydrocarbon molecules of crude oil have higher tendency to bind to the BN-coated surface than with an uncoated surface. In other words, adding h-BN to tobermorite will increase its ability to adsorb crude oil.

## 3. Conclusions

In conclusion, it has been proven that incorporation of h-BN can mechanically reinforce the cement and concrete materials while at the same time increase their efficiency to adsorb hydrocarbons such as crude oil. This opens the possibility to engineer functional concrete structures such as road pavements and water purification systems. Cement and porous concrete filled with h-BN fillers have potential environmental applications in addition to their traditional role as structural materials.

## 4. Experimental Section

*GO Preparation*: GO was prepared according to the method in ref. [13]. Using a modified Hummers method[22,23] GO was synthesized from graphite powder (50 μm mesh size, Sigma Aldrich). To achieve full oxidation of graphite powders, concentrated sulfuric acid ($H_2SO_4$, 50 mL) was heated to ≈90 °C with potassium sulfate ($K_2S_2O_8$, 10 g); phosphorous pentoxide ($P_2O_5$, 10 g) was added and the solution was stirred until all of the components were fully dissolved. After cooling the mixture to ≈80 °C, ≈12 g graphite powder was added to the solution, and the mixture was kept at ≈80 °C for ≈4.5 h. Then, the mixture was diluted with ≈2 L of deionized (DI) water and left overnight. Next day after filtering the solution by using a 0.2 μm nylon Millipore membrane, the solid was dried in air overnight. Sulfuric acid ($H_2SO_4$, 460 mL) was placed into an Erlenmeyer flask and cooled to 0 °C by an ice bath, and then pretreated graphite was added with stirring while potassium permanganate ($KMnO_4$, 60 g) was added very slowly. Note that the temperature was checked so as not to increase above ≈10 °C. After adding DI water (≈920 mL) slowly (temperature monitored to not climb above ≈50 °C using an ice bath), the solution was kept at 35 °C for 2 h and diluted with ≈2.8 L of DI water; then ≈50 mL of 30% $H_2O_2$ was subsequently added. Finally, the solution was kept for one day and then filtered and washed with 10% HCl solution, followed by DI water to remove the acid, and the resulting solid was dried in air.

*h-BN/GO Cement Composite Fabrication Process*: The commercial h-BN powders purchased from Sigma-Aldrich and dispersed in Portland cement based on the desired weight fraction of the fillers. Because the BN was not dispersible in water, a ball milling technique was used to disperse the fillers in a cement matrix. Accordingly, the h-BN powders and cement were shaken in a plastic container using steel balls (5 mm in diameter) for ≈15 min. Then, water was added (water:cement ratio was 0.33:1) and all components were mechanically mixed for ≈10 min before molding the cylindrical specimens (7 cm in diameter and 14 cm in height) for mechanical tests. To fabricate the GO/cement composite samples, since GO was dispersible in water, a high amplitude bath sonicator was used to disperse the fillers in cement matrix for ≈ 1 h. The water:cement ratio and mixing conditions were similar to those of BN/cement composites before molding the cylindrical coupons.

*h-BN/GO Concrete Composite Fabrication Process*: To fabricate the h-BN/concrete and GO/concrete specimens, above methods were utilized to disperse the h-BN and GO fillers in cement matrix except limestone aggregates was mixed with other components before molding the cylindrical specimens (12 cm in diameter and 24 cm in height). The aggregate size was ≈0.5–1.5 cm, and water-to-cement and aggregate-to-cement ratios were 1:0.33 and 5:1, respectively.

## Acknowledgements

M.A.R. and T.N.N. contributed equally to this work. P.M.A., R.V., and N.T.N. acknowledge funding from the U.S. Army Research Office MURI

grant W911NF- 11-1-0362, the U.S. Office of Naval Research MURI grant N000014-09-1-1066 on novel free-Standing 2D crystalline materials focusing on atomic layers of nitrides, oxides, and sulfides. P.M.A. and R.V. acknowledge the support provided by the Department of Energy (DOE) Grant DE-SC0001479.The authors would like to thank Dr. George Hirasaki, Department of Chemical and Biomolecular Engineering at Rice University, for supplying crude oil in this research. D.P.H is grateful to the NSF for the Graduate Research Fellowship award no. 0940902.

Received: December 28, 2012
Revised: April 11, 2013
Published online: May 27, 2013

[1] O. Stephan, P. M. Ajayan, C. Colliex, Ph. Redlich, J. M. Lambert, P. Bernier, P. Lefin, *Science* **1994**, *266*, 1683.
[2] A. Lipp, K. A. Schwetz, K. Hunold, *J. Eur. Ceram. Soc.* **1989**, *5*, 3.
[3] C. Zhi, Y. Bando, C. Tang, H. Kuwahara, D. Golberg, *Adv. Mater.* **2009**, *21*, 2889.
[4] R. T. Paine, C. K. Narula, *Chem. Rev.* **1990**, *90*, 73.
[5] H. Ishida, S. Rimdusit, *Thermochim. Acta* **1998**, *320*, 177.
[6] M. O. Adebajo, R. L. Frost, J. T. Kloprogge, O. Carmody, S. Kokot, *J. Porous Mater.* **2003**, *10*, 159.
[7] H.-M. Choi, R. M. Cloud, *Environ. Sci. Technol.* **1992**, *26*, 772.
[8] Z.-L. Xu, T.-S. Chung, Y. Huang, *J. Appl. Polym. Sci.* **1999**, *74*, 2220.
[9] J. Kong, K. Li, *Sep. Purif. Technol.* **1999**, *16*, 83.
[10] M. Cheryana, N. Rajagopalan, *J. Membr. Sci.* **1998**, *151*, 13.
[11] T. Mohammadi, M. Kazemimoghadam, M. Saadabadi, *Desalination* **2003**, *157*, 369.
[12] S. Watcharotone, A. D. Dikin, S S. Tankovich, R. Piner, I. Jung, G. H. B. Dommett, G. Evmenenko, S. Wu, S. Chen, C. Liu, S.-E. Wu, S. T. Nguyen, R. S. Ruoff, *Nano Lett.* **2007**, *7*, 1888.
[13] S. Stankovich, D. A. Dikin, G. H. B. Dommett, K. M. Kohlhaas, E. J. Zimney, E. A. Stach, R. D. Piner, S. B. T. Nguyen, R. S. Ruoff, *Nature* **2006**, *442*, 282.
[14] K. E. Prasad, B. Das, U. Maitra, U. Ramamurtya, C. N. R. Rao, *Proc. Natl. Acad. Sci. USA* **2009**, *106*, 13186.
[15] L. S. Walker, V. R. Marotto, M. A. Rafiee, N. Koratkar, E. L. Corral, *ACS Nano* **2011**, *5*, 3182.
[16] N. G. Chopra, A. Zettl, *Solid State Commun.* **1998**, *105*, 297.
[17] M. S. R. N. Kiran, K. Raidongia, U. Ramamurty, C. N. R. Rao, *Scr. Mater.* **2011**, *64* 592.
[18] J. Yang, G. Jiang, *Cement Concrete Res.* **2003**, *33*, 381.
[19] R. Hathcock, K. Koerner, T. Hughes, D. Kundu, J. López de Cárdenas, C. West, *Oilfield Rev.* **2006**, *18*, *2006*, 34.
[20] S. Gilje, S. Han, M. Wang, K. L. Wang, R. B. Kaner, *Nano Lett.* **2007**, *7*, 3394.
[21] N. I. Kovtyukhova, P. J. Ollivier, B. R. Martin, T. E. Mallouk, S. A. Chizhik, E. V. Buzaneva, A. D. Gorchinskiy, *Chem. Mater.* **1999**, *11*, 771.
[22] W. S. Hummers, R. E. Offeman, *J. Am. Chem. Soc.* **1958**, *80*, 1339.
[23] K. N. Kudin, B. Ozbas, H. C. Schniepp, R. K. Prud'homme, I. A. Aksay, R. Car, *Nano Lett.* **2008**, *8*, 36.
[24] C. Wang, Y. Huang, Q. Zan, L. Zou, S. Cai, *J. Am. Ceram. Soc.* **2002**, *61*, 2457.
[25] B. O. Brattebo, D. B. Booth, *Water Res.* **2003**, *37*, 4369.
[26] H. F. W. Taylor, *J. Am. Ceram. Soc.* **1986**, *69*, 464.
[27] H. Matsuyama, J. F. Young, *Chem. Mater.* **1999**, *11*, 16.
[28] M. L. D. Gougar, B. E. Scheetz, D. M. Roy, *Waste Manag.* **1996**, *16*, 295.
[29] D. C. Villalanti, J. C. Raia, J. B. Maynard, in *Encyclopedia of Analytical Chemistry* (Ed: R. A. Meyers) John Wiley and Sons Ltd., Chichester, UK **2000**, pp. 6726-6741.
[30] C. A. Hughey, R. P. Rodgers, A. G. Marshall, *Anal. Chem.* **2002**, *74*, 4145.
[31] R. Shahsavari, R. J. M. Pellenq, F.-J. Ulm, *Phys. Chem. Chem. Phys.* **2011**, *13*, 1002.
[32] W. D. Cornell, P. Cieplak, C. I. Bayly, I. R. Gould, K. M. Merz, D. M. Ferguson, D. C. Spellmeyer, T. Fox, J. W. Caldwell, P. A. Kollman, *J. Am. Chem. Soc.* **1995**, *117*, 5179.
[33] J. R. Maple, U. Dinur, A. T. Hagler, *Proc. Natl. Acad. Sci. USA* **1988**, *85*, 5350.
[34] W. G. Hoover, *Phys. Rev. A.* **1985**, *31*, 1695.
[35] J. P. Hansen, I. R. McDonald *Theory of Simple Liquids*. Academic Press, London **1986**.
[36] W. Humphrey, A. Dalke, K. Schulten, *J Mol. Graph.* **1996**, *14*, 33.